Estimation of Secondary Organic Aerosol Viscosity from Explicit Modeling of Gas-Phase Oxidation of Isoprene and α-pinene

Tommaso Galeazzo[1], Richard Valorso[2], Ying Li[1], Marie Camredon[2], Bernard Aumont[2], Manabu Shiraiwa[1,*]

1. Department of Chemistry, University of California, Irvine, CA92625, USA

2. Laboratoire Interuniversitaire des Systèmes Atmosphérique (LISA), UMR 7583, Université Paris-Est Créteil, CNRS, Université de Paris, Institut Pierre Simon Laplace (IPSL), Créteil, France

* Correspondence to: m.shiraiwa@uci.edu

Abstract.

Secondary organic aerosols (SOA) are major components of atmospheric fine particulate matter, affecting climate and air quality. Mounting evidence exists that SOA can adopt glassy and viscous semisolid states, impacting formation and partitioning of SOA. In this study, we apply the GECKO-A (Generator of Explicit Chemistry and Kinetics of Organics in the Atmosphere) model to conduct explicit chemical modeling of isoprene photooxidation and α-pinene ozonolysis and their subsequent SOA formation. The detailed gas-phase chemical schemes from GECKO-A are implemented into a box model and coupled to our recently-developed glass transition temperature parameterizations, allowing us to predict SOA viscosity. The effects of chemical composition, relative humidity, mass loadings and mass accommodation on particle viscosity are investigated in comparison with measurements of SOA viscosity. The simulated viscosity of isoprene SOA agrees well with viscosity measurements as a function of relative humidity, while the model underestimates viscosity of α-pinene SOA by a few orders of magnitude. This difference may be due to missing processes in the model including autoxidation and particle-phase reactions leading to the formation of high molar mass compounds that would increase particle viscosity. Additional simulations imply that kinetic limitations of bulk diffusion and reduction in mass accommodation coefficient may play a role in enhancing particle viscosity by suppressing condensation of semi-volatile compounds. The developed model is a useful tool for analysis and investigation of the interplay among gas-phase reactions, particle chemical composition and SOA phase state.

1. Introduction

Secondary organic aerosols (SOA) are ubiquitous in the atmosphere and represent a major component of fine particulate matter, affecting air quality, climate and public health (Jimenez et al., 2009; Pöschl & Shiraiwa, 2015). Due to their complexity, SOA represent a large source of uncertainty in current understanding of global climate change and air pollution (Tsigaridis et al., 2014; Ciarelli et al., 2019). Development of SOA models represents one of the most challenging and demanding problems in atmospheric chemistry (Shrivastava et al., 2017). Formation of SOA is initiated by gas-phase oxidation of biogenic and anthropogenic volatile organic compounds (VOC) (Kroll and Seinfeld, 2008). Typically, multigenerational oxidation of VOC in the gas phase leads to the formation of a myriad of semi-volatile and low volatility compounds which can condense on pre-existing particles (Ziemann and Atkinson, 2012; Noziere et al., 2015) or contribute to nucleation and new particle formation (Tröstl et al., 2016). As gas-phase oxidation is a driving step of SOA formation, there is a strong need for a computational tool that can generate exhaustive gas-phase chemical mechanisms. The GECKO-A (Generator of Explicit Chemistry and Kinetics of Organics in the Atmosphere) model is to-date the most extensive generator of gas-phase chemical schemes; based on established reaction pathways and structure-activity relationships, it automatically generates detailed gas-phase mechanisms involving thousands-to-millions of oxidation products from a given VOC precursor (Aumont et al., 2005; Aumont et al., 2012; Lee-Taylor et al., 2011).

Most aerosol models treat SOA particles as homogeneous and well-mixed liquids with a dynamic viscosity (η) below 10^2 Pa s. Recent studies provide accumulating evidence that SOA can adopt glassy solid ($\eta \geq 10^{12}$ Pa s) or amorphous semi-solid phase states ($10^2 \leq \eta < 10^{12}$ Pa s) depending on chemical composition, relative humidity (RH), and temperature (Koop et al., 2011; Reid et al., 2018; Virtanen et al., 2010). The particle phase state is impacted by SOA chemical composition, hygroscopicity and water content, as water can act as a plasticizer lowering SOA viscosity (Mikhailov et al., 2009). It has been observed that ambient SOA particles can bounce off from an impactor stage depending on ambient conditions, indicating non-liquid states of organic particles (Virtanen et al., 2011; Bateman et al., 2017; Slade et al., 2019). Measurements of the viscosity of SOA bulk materials derived from the oxidation of limonene (Hinks et al., 2016), toluene (Song et al., 2016a), α-pinene (Renbaum-Wolff et al., 2013; Kidd et al., 2014; Bateman et al., 2015; Zhang et al., 2015; Grayson et al., 2016; Hosny et al., 2016) and isoprene (Song et al., 2015) have confirmed that viscosity of SOA particles can vary depending on temperature and RH (Petters et al., 2019). In addition, previous studies

69   have shown that SOA chemical composition can be affected by experimental conditions upon
70   SOA formation such as RH and particle mass concentrations (Kidd et al., 2014; Hinks et al.,
71   2018; Grayson et al., 2016; Jain et al., 2018). These results imply that SOA viscosity and phase
72   state are dynamic properties in response to chemical processing of organic aerosols and
73   variations in RH and temperature in the atmosphere.

74   In liquid particles, molecules diffuse quickly in the particle bulk, leading to rapid
75   establishment of gas-particle equilibrium. In glassy and viscous particles, kinetic limitations of
76   bulk diffusion can significantly retard gas-particle partitioning, prolonging equilibration
77   timescales (Li and Shiraiwa, 2019; Mai et al., 2015; Vaden et al., 2011), while relatively fast
78   particle-particle mixing were observed at intermediate and high RH (Ye et al., 2016; 2018).
79   Model simulations suggest that an assumption of instantaneous equilibrium partitioning can
80   result in substantial overestimation of particle mass concentration and underestimation of gas-
81   phase mass concentration (Shiraiwa and Seinfeld, 2012). A proper consideration of particle
82   phase state is essential for simulating particle size distribution dynamics in SOA growth
83   (Shiraiwa et al., 2013; Zaveri et al., 2018; Zaveri et al., 2020). Heterogeneous and multiphase
84   reactions (Kuwata and Martin, 2012; Shiraiwa et al., 2011; Davies & Wilson, 2015; Zhang et
85   al., 2018; Marshall et al., 2018; Zhou et al., 2019) as well as activation to cloud droplets and
86   ice crystals (Slade et al., 2017; Knopf et al., 2018) can also be impacted by glassy and
87   amorphous semisolid states. Thus, it is important to consider the effects of particle phase state
88   on SOA processes for accurate representation of the fate of SOA particles in aerosol models.

89   Recently, we have developed parameterizations to predict glass transition temperature
90   (T_g) of organic compounds based on molar mass and atomic O:C ratio (Shiraiwa et al., 2017),
91   elemental composition (i.e., number of carbon, hydrogen, oxygen, nitrogen, and sulfur atoms)
92   (DeRieux, et al., 2018), and volatility (Li et al., 2020). T_g is a characteristic temperature at
93   which a phase transition from a glassy solid state to an amorphous semi-solid state occurs (Koop
94   et al., 2011). Applying the Gordon-Taylor mixing rule for mixtures of SOA multiple
95   components and water, the viscosity of SOA can be estimated by the T_g-scaled Arrhenius plot
96   of viscosity (DeRieux, et al., 2018). This method has been successfully applied to estimate
97   particle viscosity based on elemental composition obtained from high resolution mass
98   spectrometry (Schum et al., 2018; Ditto et al., 2019; Song et al., 2019). Gervasi et al. (2020)
99   simulated viscosity of aqueous SOA surrogate mixtures derived from oxidation of α-pinene,
100 isoprene and toluene using the AIOMFAC-VISC model combined with the T_g parametrization
101 of DeRieux et al (2018), demonstrating the capability and flexibility of the group-contribution
102 method in predicting the viscosity for organic mixtures of varying degrees of complexity.

103   There is a strong need for the development of a modelling tool for further elucidation
104   of the impacts of various aerosol properties and processes on particle viscosity. A better
105   understanding of the interplay among gas-phase reactions, chemical composition and viscosity
106   of SOA is essential for further development of model representation of the evolution of SOA
107   in the atmosphere. In this study, the T_g and viscosity prediction methods are implemented into
108   the GECKO-A and box model. Model simulations with explicit chemical mechanisms are
109   conducted to reproduce chamber experimental conditions for SOA generation and subsequent
110   viscosity measurements. The effects of chemical composition and mass accommodation on
111   SOA partitioning and viscosity are also investigated. The objective of this work is to develop a
112   useful tool for analysis and investigation of SOA chemical composition and phase state and to
113   expand our fundamental understanding on such properties.

114
115   **2. Methods**
116   **2.1. GECKO-A**
117   GECKO-A generates detailed gas-phase chemical oxidation schemes and the associated
118   gas-particle mass transfers for SOA formation. It produces explicit highly detailed chemical
119   mechanisms starting from experimental data and structure-activity relationships (SARs)
120   (Aumont et al., 2005). Implemented into a box model, these explicit chemical mechanisms
121   simulate the oxidation of parent VOC precursors to oxidation products, their subsequent gas-
122   phase chemistry, as well as partitioning into the particle phase based on their vapor pressures
123   (Camredon et al., 2007). GECKO-A is frequently updated to include the newly discovered
124   chemical processes in the mechanism generator: recently, the mechanism generator has been
125   extended to treat the chemistry of aromatic organic compounds based on the latest SAR
126   developments (Jenkin et al., 2018a; Jenkin et al., 2018b; Jenkin et al., 2019; Jenkin et al., 2020).
127   Other recent updates include the chemistry of cyclic structures (Valorso et al., 2011), the gas-
128   aqueous phase partitioning (Mouchel-Vallon et al., 2013), and the gas to chamber wall
129   partitioning (La et al., 2016). The chemical mechanism does not account for gas-phase
130   chemistry of species with vapor pressure below 10^{-13} atm, which are assumed to be of enough
131   low volatility to partition to the condensed phase. In our simulations, species vapor pressures
132   are estimated via the approach by Nannoolal et al. (2008).
133   The mechanism generator follows a reduction protocol optimizing the number of
134   generated reactions and chemical species (Valorso et al., 2011). This protocol has been
135   established to reduce the computational cost of box-model simulations. In the gas phase, isomer
136   substitution is not allowed for position isomers when the overall yield for the product is > 5%;

137 otherwise only the highest-yield positional isomer is considered. For each reaction, pathways

138 with branching ratios < 5% are not accounted for and the main reaction branches are scaled

139 proportionally (Valorso et al., 2011). The chemical mechanism accounts for chemistry of

140 peroxy and alkoxy radicals generated during precursors oxidation. SOA chemistry is a multi-

141 generational process and the generated chemical schemes follow the chemistry of reaction

142 products up to the 5th generation in our simulations. The GECKO-A version used in this study

143 has been recently enriched with SARs estimations of alkoxy radical decomposition and H-

144 migration reaction rates (Vereecken and Peeters, 2009; La et al., 2016). Rate coefficients and

145 branching ratios for gas-phase reactions of OH with aliphatic compounds and peroxy radicals

146 are estimated based on recent SAR investigations (Jenkin et al., 2018a,b). Our simulations do

147 not include autoxidation and condensed-phase chemistry, which represent limitations of

148 GECKO-A modeling.

149   α-pinene and isoprene oxidation mechanisms have been investigated extensively both

150 in model and experimental studies. Their oxidation mechanisms are well known, providing

151 good estimations of resulting SOA composition. The SARs for both α-pinene and isoprene

152 oxidation are implemented into GECKO-A with state-of-the-art protocols estimating radical

153 reactions and respective rate constants. The base mechanism for α-pinene photooxidation and

154 ozonolysis include a detailed description of reactions with OH radicals (McVay et al., 2016),

155 and branch reactions identified via quantum and theoretical chemical calculations (Peeters et

156 al., 2001; Vereecken et al., 2007). Stabilized Criegee intermediates (SCIs) chemistry is not

157 treated explicitly and stable products are directly assigned via a rule-base method. This scheme

158 accounts for a direct reaction route to account for pinonaldehyde formation during the reaction

159 of SCIs with water (McVay et al., 2016).

160   α-pinene GECKO-A mechanisms were evaluated in previous studies by comparisons

161 with chamber experiments of SOA formation from photo-oxidation (Valorso et al. 2011,

162 McVay et al., 2016) and ozonolysis (Denjean et al., 2015). The model captures the qualitative

163 features of SOA formation with the variation of NOx levels during photolysis experiments, and

164 with temperature for ozonolysis experiments. The measured SOA mass was overestimated by

165 the model in Valorso et al. (2011) and Denjean et al. (2015), which could be in part explained

166 by the loss of low volatile organic compounds onto the chamber wall (McVay et al., 2016; La

167 et al., 2016). In addition, McVay et al (2016) highlighted a possible overestimation of the

168 simulated contribution of later-generation oxidation products to SOA mass at high OH levels,

169 and an underestimation of the SOA growth at low OH levels that could be due to lack of

170 autoxidation processes in the mechanisms generated with GECKO-A. The influence of these
171 limitations on the results simulated here are discussed along the paper. The GECKO-A isoprene
172 oxidation scheme follows the main protocol developed by Aumont et al. (2005) and branching
173 reactions for isoprene + OH are also considered (Paulot et al., 2009). Isoprene mechanisms
174 generated with GECKO-A is for the first time indirectly evaluated in this study. The chemical
175 schemes for α-pinene and isoprene oxidation are composed of 84,000 and 1,900 species, and
176 of ~700,000 and ~17,000 reactions, respectively.

177

178 **2.2. Box model and simulations setup**

179 Each chemical mechanism is coupled to a box model representing SOA formation from
180 α-pinene or isoprene oxidation in specific chamber experiments. The time evolution of species
181 concentration is computed through a two-step method that explicitly solves stiff ordinary
182 differential equations (Verwer et al., 1994; 1996). The experimental conditions are summarized
183 in **Table 1**. All laboratory experiments were performed in absence of seed particles, but the box
184 model used in our simulations does not treat nucleation. Thus, in our simulations the first steps
185 of nucleation are approximated by the addition of seed particles with a particle radius of 5 nm
186 and a concentration of 10^4 particles cm^{-3} (McVay et al., 2016). The particle number
187 concentration is assumed to remain constant during simulations (coagulation is not treated),
188 while the particle radius evolves following the partitioning of organics. The density of SOA
189 particles is assumed to be 1.2 g cm^{-3} (Kuwata et al., 2012). All simulations are conducted with
190 a NOx mixing ratio of 3 ppt to reflect low NOx conditions of chamber and flow tube
191 experiments. For all simulations we consider reversible gas-wall partitioning of organic species
192 with the vapor wall loss rate of of 10^{-3} s^{-1} based on experimental observations (Lim and
193 Ziemann, 2009, McVay et al., 2016). Photolysis rates are computed using the cross-sections
194 and the quantum yields from Aumont et al. (2005). Photolysis conditions are set to average
195 daylight conditions of a mid-latitude spring day for isoprene photooxidation simulations and to
196 zero for α-pinene dark ozonolysis experiments, coherent with the experimental conditions.

197 For continuous flow reactor experiments, the concentrations of VOC precursors and
198 oxidants were stable by continuous inflow and outflow of gases from the tube reactor; in the
199 box model simulations precursor concentrations are fixed at steady state values as measured in
200 corresponding experiments. In chamber batch experiments, the reactants were injected once at
201 the beginning of the experiment and the concentrations evolved; in box model simulations the
202 VOC precursor and ozone concentrations are initially set to the respective experimental values

203 and species concentrations evolve due to gas oxidation, gas-particle partitioning, and wall

204 deposition. SOA particles were formed under dry conditions and then exposed to water vapor

205 at different RH for viscosity measurements; the same procedure is applied in our simulations

206 by forming SOA at RH = 0.5% and then viscosity estimations are conducted by considering

207 hygroscopic growth at elevated RH. For each set of simulations, the measured RH and

208 temperature were used to constrain the simulation conditions. Note that partitioning of water is

209 not considered in the box model as particle water uptake should be very minor under the very

210 low RH values at which SOA particles were formed.

211   The box model treats the mass transfer of gaseous organic species to particles and to

212 chamber walls. Gas-particle partitioning is assumed to follow Raoult's law at equilibrium (La

213 et al., 2016) (i.e., depending on the saturation vapor pressure of the organic compounds

214 assuming ideal mixing). Gas to particle partitioning is described in the box model using the gas-

215 particle mass transfer coefficient of a compound (k_{gp} in s^{-1}) with the Fuchs-Sutugin approach in

216 the transition regime as (Seinfeld and Pandis, 2016):

217

218
$$k_{gp} = 4\pi D_g\, r_P\, N_P\, \beta \tag{1}$$

219

220
$$\beta = \frac{0.75\,\alpha\,(1+Kn)}{Kn^2 + Kn + 0.283\,Kn\,\alpha + 0.75\alpha} \tag{2}$$

221

222   where D_g (cm^2 s^{-1}) is the gas diffusivity, r_p (cm) is the particle radius, N_p (cm^{-3}) is the

223 particle number concentration, K_n is the Knudsen number, and α is the mass accommodation

224 coefficient. α, also termed as the bulk accommodation coefficient, represents the probability

225 for a gas molecule colliding with surface to enter the bulk of the particle. Based on recent

226 experiments and molecular dynamics simulations α is assumed to be unity for the base case

227 scenario of our simulations (Liu et al., 2019; Julin et al., 2014). This approach does not account

228 for potential kinetic limitations caused by bulk diffusion in viscous particles.

229   A recent study has introduced an effective mass accommodation coefficient α_{eff}, which

230 effectively considers the kinetics of accommodation at the surface, transfer across the gas-

231 particle interface, and further transport into the particle bulk (Shiraiwa and Pöschl, 2020):

232

233
$$\alpha_{eff} = \alpha_s \frac{1}{1 + \frac{\alpha_s\,\omega\,C^0}{4\,D_b\,\rho_p}\frac{r_p}{5}\cdot 10^{-12}\frac{\text{g cm}^{-3}}{\mu\text{g m}^{-3}}} \tag{3}$$

234

235   where α_s is the surface accommodation coefficient (i.e., the probability for a gas

236   molecule colliding with surface to adsorb on the particle surface), ω (cm s^{-1}) is the mean thermal

237   velocity of the organic compound in the gas phase, D_b (cm^2 s^{-1}) is diffusivity in the condensed

238   phase, ρ_p (g cm^{-3}) is the particle density, and C^0 (µg m^{-3}) is the pure compound saturation mass

239   concentration. Application of α_{eff} in the Fuchs-Sutugin approach (e.g., $\alpha = \alpha_{eff}$) yields SOA

240   partitioning with effective consideration of kinetic limitations induced by slow bulk diffusion

241   in viscous particles. This approach can yield consistent results with a detailed kinetic multilayer

242   model (KM-GAP, Shiraiwa et al., 2012) and two-film model solutions (Zaveri et al., 2014). We

243   implement this method to explore the effects of mass accommodation and kinetic partitioning

244   on predicted viscosity by comparing with the base case scenario (e.g., α fixed to 1).

245
246   **2.3. Viscosity prediction implementation**

247   The glass transition temperature of an organic compound i ($T_{g,i}$) can be estimated with

248   the following recently-developed parameterization based on its elemental composition

249   (DeRieux et al., 2018):

250

251    $T_{g,i} = (n_C^0 + \ln(n_C))\, b_C + \ln(n_H)\, b_H + \ln(n_C)\ln(n_H)\, b_{CH} + \ln(n_O)\, b_O + \ln(n_C)\ln(n_O)\, b_{CO}$ (4)

252

253   Where the coefficient values for [n_C^0, b_C, b_H, b_{CH}, b_O, and b_{CO}] are [1.96, 61.99, -113.33, 28.74,

254   0, 0] for CH compounds and [12.13, 10.95, -41.82, 21.61, 118.96, -24.38] for CHO compounds.

255   We have also included the recently developed parametrization for CHON compounds by Li et

256   al. (2020):

257

258    $T_{g,i} = (n_C^0 + \ln(n_C))\, b_C + \ln(n_O)\, b_O + \ln(n_N)\, b_N + \ln(n_C)\ln(n_O)\, b_{CO} + \ln(n_C)\ln(n_N)\, b_{CN} + \ln(n_O)\ln(n_N)$

259   b_{ON} (5)

260

261   Where the coefficient values for [n_C^0, b_C, b_O, b_N, b_{CO}, b_{CN}, and b_{ON}] are [5.34, 31.53, -7.06,

262   134.96, 6.54, -34.36, and -15.35]. These parametrizations can predict $T_{g,i}$ with an uncertainty

263   of about ±30 K; note that, however, in multicomponent SOA mixtures this uncertainty would

264   be much smaller for ideal mixing conditions (Shiraiwa et al., 2017; DeRieux et al., 2018; Li et

265   al., 2020). The T_g of a mixture of organic compounds (e.g. dry SOA) can be estimated using

266   the Gordon-Taylor equation with a Gordon-Taylor constant (k_{GT}) of 1: $T_{g,org} = \sum_i \omega_i T_{g,i}$, where

267   ω_i is the mass fraction of compound i (Dette et al., 2014).

268   The Gordon-Taylor equation can also be used to estimate the glass transition

269   temperature of mixtures of organic compounds and water ($T_g(w_{org})$):

270

271
$$T_g(w_{org}) = \frac{(1-w_{org})T_{g,w} + \frac{1}{k_{GT}}w_{org}T_{g,org}}{(1-w_{org}) + \frac{1}{k_{GT}}w_{org}}$$
(5)

272

273   where w_{org} is the mass fraction of organics, $T_{g,w}$ is the glass transition temperature of pure water

274   (136 K), and k_{GT} is the Gordon-Taylor constant which is assumed to be 2.5 (Koop et al., 2011;

275   Zobrist et al., 2008). The w_{org} is calculated using the mass concentration of water (m_{H_2O}) and of

276   the organics in SOA (m_{SOA}) as: $w_{org} = m_{SOA} / (m_{SOA} + m_{H_2O})$. m_{H_2O} can be calculated using the

277   Kohler theory with effective hygroscopicity parameter (κ) (Petters and Kreidenweis, 2007).

278   Once $T_g(w_{org})$ has been computed, the viscosity (η) can be derived with the following

279   equation based on the Vogel-Tammann-Fulcher approach (DeRieux et al., 2018):

280

281
$$\log \eta = -5 + 0.434 \frac{T_0\, D}{T - T_0}$$
(7)

282

283
$$T_0 = \frac{39.17\; T_g(w_{org})}{D + 39.17}$$
(8)

284

285   where T_0 is the Vogel temperature and D is the fragility parameter. The D value is assumed to

286   be 10 based on previous studies (Shiraiwa et al., 2017; DeRieux et al., 2018).

287   Viscosity can then be converted into bulk diffusivity using the Stokes-Einstein equation:

288

289
$$D_b = \frac{kT}{6\pi a \eta}$$
(9)

290

291   where k is the Boltzmann constant (1.38×10^{-23} J K^{-1}), T is the temperature (K), and a is the

292   effective molecular radius (m). This relation, however, may not be accurate for very high

293   viscosities and needs to be corrected with the fractional Stokes-Einstein (FSE) relation (Evoy

294   et al., 2019):

295
$$D_b = D_{b,c} \left(\frac{\eta_c}{\eta}\right)^{\xi}$$
(10)

296

297 where ξ is an empirical fit parameter with the value of 0.93 (Evoy et al., 2019), η_c is the

298 crossover viscosity with the value of 10^{-3} Pa s, and $D_{b,c}$ is the crossover diffusion coefficient at

299 $\eta_c = 10^{-3}$ Pa s as determined by the Stokes-Einstein equation (Eq. 9).

300 For validation and applicability of T_g parameterizations and the viscosity prediction

301 method, they have been applied to high resolution mass spectrometry data of toluene SOA and

302 biomass burning aerosols (DeRieux et al., 2018), SOA generated by diesel fuels (Song et al.,

303 2019), β-Caryophyllene SOA (Maclean et al., 2021), and surrogate VOC mixtures by healthy

304 and stressed plants (Smith et al., 2021), agreeing well with viscosity measurements.

305

306 **3. Results and discussion**

307 **3.1 Viscosity predictions of isoprene and α-pinene SOA**

308 Figure 1 shows the measured and simulated viscosities of isoprene SOA, showing a

309 very good agreement with experimental observations. SOA generated by isoprene ozonolysis

310 adopt a semi-solid state for RH < 40% and a liquid state for RH > 60%. The model predicted

311 $T_{g,org}$ is 260 K, which is in agreement with a previous estimation of 255 K (Berkemeier et al.,

312 2014). All simulated viscosities with $\kappa = 0.1$ fall within uncertainties of experimental

313 measurements except at 70% RH, which is slightly below the lower bound of the error bar of

314 experimental measurements. The simulated O:C ratio is 1.0, which is within the range of their

315 estimation of 0.64-1.1 based on previous chamber experiments (Song et al., 2015). To examine

316 the effects of κ on the calculated viscosity of isoprene SOA, sensitivity studies are conducted

317 by varying κ within the range of 0.05–0.15, showing that lower and higher κ would lead to

318 higher and lower viscosity, respectively.

319 Isoprene photooxidation in chamber experiments was conducted with very high

320 precursor concentrations and a short reaction time such that a traditional gas-phase oxidation

321 scheme dominates, which can be captured well in GECKO-A (Aumont et al., 2005). Note that

322 the formation of isoprene epoxydiols (IEPOX) (Paulot et al., 2011; Bates et al., 2014) and

323 subsequent uptake of IEPOX into acidic particles followed by a series of multiphase reactions

324 including the formation of oligomers and organosulfates (Riva et al, 2019) are found to be

325 important in the ambient atmosphere (Wennberg et al., 2018). The uptake of IEPOX can be

326 limited by bulk diffusion in a viscous matrix (Zhang et al., 2018) and IEPOX-SOA is reported

327 to have high viscosity (Riva et al., 2019). For viscosity simulations of atmospherically relevant

328 IEPOX-derived SOA, IEPOX multiphase processes would need to be treated in future studies.

329   Figure 2 shows viscosity of α-pinene SOA measured in a number of studies and the
330   corresponding simulated results by the GECKO-A box model for each experimental condition.
331   Based on previous laboratory measurements κ was assumed to be 0.1 (Lambe et al., 2011b;
332   Pajunoja et al., 2015; Petters et al., 2019). Overall, the model simulations can reproduce the
333   RH-dependent viscosity of α-pinene SOA, showing that α-pinene SOA is semi-solid between
334   0-65% RH and liquid for RH > 65% at the room temperature. Simulated viscosity values of α-
335   pinene SOA are by a few orders of magnitude higher than the ones simulated for isoprene SOA,
336   which is consistent with experimental observations. Simulation results for Renbaum-Wolff's
337   and Grayson's experiments fall within the relatively large uncertainties of experimental
338   measurements for the 40-60% RH range. In simulations for Renbaum-Wolff's experiments at
339   RH > 60%, the predicted viscosity values are about one order of magnitude lower than the
340   measured values. Larger deviations are observed for RH < 40%, where simulated viscosities
341   are up to four orders of magnitude lower than experimental measurements. The simulated
342   viscosities are about one order of magnitude higher than Graysons's measurements for 20 < RH
343   < 40%. The simulated viscosity for Bateman's experiment agrees well with the observed
344   experimental value within uncertainties.

345   Kidd et al. (2014) provided only one data point at 85% RH, which also represents
346   inferred viscosity based on their impactor measurement; the predicted viscosity is three orders
347   of magnitude below the inferred value, but only one order of magnitude below its lower bound.
348   For simulations of Zhang et al. (2015) our predictions are about three to four orders of
349   magnitude lower than measurements.

350   The simulated $T_{g,org}$ are within 255-285 K (see Table 1), which is in good agreement
351   with a previous estimation of 278 K (Berkemeier et al., 2014) and a measurement of 272 K
352   (Petters et al., 2019). To assess overall performance of our viscosity predictions, measured and
353   simulated viscosities were fitted respectively with a second-order polynomial regression. While
354   the RH dependence of viscosity is very well captured by our simulations, the simulated values
355   underestimate viscosity by about two or three orders of magnitude on average. The variance of
356   model simulations and experimental measurements calculated for the logarithm of the viscosity
357   are very similar (R^2 = 0.85), indicating that the GECKO-A box model can reproduce the
358   variability observed in experimental measurements with different experimental conditions.

359   Grayson et al. (2016) investigated the impact of SOA mass loadings on viscosity,
360   observing lower viscosity with higher SOA mass concentrations in the range of 10^2-10^4 µg m$^-$
361   ^{3}. We conducted four different simulations where precursor concentrations were varied in the

362   range of the experimental values to match the final SOA mass loadings. As shown in Fig. 3,

363   our simulated viscosities are within the experimental uncertainties, capturing this dependence

364   very well. At higher mass loadings, compounds with relatively high volatility and low T_g can

365   condense on particles, leading to a reduction of SOA viscosity; for lower mass loadings,

366   condensation of lower volatility compounds with higher T_g would be dominant, resulting in

367   higher viscosity.

368

369   **3.2. Chemical composition and functional group distributions of SOA**

370   The GECKO-A box model tracks the concentrations of species both in the gas and

371   particle phases, while retaining information on molecular properties including molar mass, O:C

372   ratio, vapor pressure, and volatility or pure compound saturation mass concentration (C_0).

373   Figure 4 shows most abundant particle-phase 500 compounds in simulated isoprene and α-

374   pinene SOA products in the 2-dimensional volatility basis set framework of O:C ratio vs. log

375   C_0 (Donahue et al., 2011). The markers are color-coded with T_g and the marker size is scaled

376   with particle-phase concentration in each simulation. Compounds with lower volatility tend to

377   have higher O:C ratio and higher T_g, in good agreement with recent experimental and model

378   studies (Zhang et al., 2019; Li et al., 2020). Isoprene oxidation products are found to have

379   higher O:C ratio, while α-pinene oxidation products have lower C_0 and higher T_g. These results

380   are in line with higher viscosity of α-pinene SOA compared to isoprene SOA, as measured and

381   modeled in Figs. 1 and 2.

382   None of these experimental studies measured average O:C ratio of SOA particles, but

383   some of them reported estimated O:C ratios based on previous experiments with similar

384   experimental conditions. Song et al. (2015) estimated the O:C ratio of isoprene SOA to be 0.64

385   -1.1, which is consistent with our simulated O:C ratio of 1.0. Renbaum-Wolff et al. (2013)

386   estimated O:C ratio of α-pinene SOA to be 0.3 – 0.4, which is slightly lower than our simulated

387   value of 0.49. Valorso et al. (2011) reported that the GECKO-A box model tends to

388   overestimate the O:C ratio of SOA generated by α-pinene photooxidation. Denjean et al. (2015)

389   showed that the O:C ratio of SOA simulated with GECKO-A from α-pinene ozonolysis was

390   coherent with the one simulated with the Master Chemical Mechanism, and within the

391   uncertainty range of the experimental value. A recent study by Gervasi et al. (2020), which

392   selected 14-21 representative reaction products based on the Master Chemical Mechanism to

393   simulate viscosity of the same measurement dataset, estimated the O:C ratio to be 1.1 for

394   isoprene SOA and 0.51 for α-pinene SOA. Overall, the O:C ratios simulated by the GECKO-

395 A box model are reasonable and in line with available measurements and modeling studies,
396 while further studies are warranted for simultaneous measurements of O:C ratio and viscosity
397 along with model applications.

398    Our method to estimate T_g of organic compounds and SOA viscosity are based on
399 elemental composition without accounting for molecular structure and specific intramolecular
400 interactions. Some organic compounds with reactive functional groups may undergo particle-
401 phase reactions, which are not treated in our simulations. To explore these aspects, we
402 investigate the functional groups distributions computed by GECKO-A and box modeling. The
403 simulated functionality group distributions of particle-phase SOA compounds are shown in Fig.
404 5. Isoprene SOA is characterized by high concentrations of alcohols (–ROH) and
405 hydroperoxides (–ROOH), followed by lower concentrations of ketones (–RC(O)R), and
406 aldehydes (–RCHO). Our results are consistent with experimental measurements showing that
407 polyols and organic peroxides are the primary species formed upon isoprene photooxidation
408 under low NOx conditions (Surratt et al., 2006). Most experiments for α-pinene led to similar
409 chemical composition with high concentrations of–RC(O)R and–ROOH, followed by slightly
410 lower concentrations of –RCHO, –ROH and carboxylic acids (–RC(O)OH). The simulations
411 for Grayson's experiments are characterized by the highest concentrations of –ROOH and –
412 ROH, and by lower fractions of –RCHO. The simulations for Kidd's experiments show the
413 second highest abundance of –ROH and noticeable amounts of –RC(O)OR. The simulation for
414 Bateman's experiment is characterized by high –RC(O)R abundance. A previous study
415 suggested that the hydrogen-bond formation among organic compounds in the SOA organic
416 matrix may influence the viscosity of α-pinene SOA significantly (Kidd et al., 2014). It has
417 been further shown that alcohol and carboxylic acid groups can increase viscosity due to the
418 formation of hydrogen bonding and ionic interactions if carboxylic acids are dissociated
419 (Grayson et al., 2017; Rothfuss and Petters, 2017). These effects are not explicitly considered
420 in our viscosity estimation method, which may be one of the reasons for the discrepancies
421 between measurements and simulations of SOA viscosity.

422    Chemical composition simulated for Zhang's experiments is characterized by the
423 highest –RCHO fraction among all experiments, which may explain the largest difference
424 between predicted and measured viscosities. Aldehydes are known to be highly reactive in the
425 condensed phase by reacting with alcohols and hydroperoxides to form peroxyhemiacetals and
426 oligomers (Ziemann and Atkinson, 2012). Such multiphase reactions could be accelerated
427 under acidic conditions in the presence of carboxylic acids (Bakker-Arkema and Ziemann,
428 2020; Shiraiwa et al., 2013). In addition, the GECKO-A model treats neither autoxidation to

429 form highly oxygenated organic molecules (HOMs) nor gas-phase dimerization reactions of

430 peroxy radicals, which are recently found to play a significant role in SOA formation and

431 growth (Bianchi et al., 2019). These higher molar mass compounds with very low volatility

432 have higher T_g, hence leading to higher SOA viscosity (Koop et al., 2011; Zhang et al., 2019;

433 Champion et al., 2019; Li et al., 2020). While the extent of effects of these processes may vary

434 among reaction conditions applied in each experiment, the lack of treatment of these processes

435 may be another plausible reason of lower simulated viscosity compared to experimental

436 measurements.

437

438 **3.3. Effects of mass accommodation**

439   All the above simulations were conducted with mass accommodation coefficient equal

440 to unity. Hereby, we investigate potential kinetic limitations of bulk diffusion on SOA

441 partitioning and resulting viscosity by simulating two distinct experimental conditions of flow

442 tube experiments by Renbaum-Wolff et al. (2013) and batch experiments by Kidd et al. (2014).

443 The effective mass accommodation coefficient (α_{eff}) is computed with Eq. 3, which is

444 implemented into Eq. 1 and 2 to simulate partitioning that effectively accounts for kinetic

445 limitations of bulk diffusion.

446   Figure 6 shows the simulated viscosity estimations for SOA formation under dry

447 conditions followed by water exposure at different RH. Final viscosity values are higher for

448 simulations with α_{eff} compared to those with α fixed to 1. For simulations of Renbaum-Wolff's

449 experiments there is very small difference in viscosity between the two simulations. For

450 simulations of Kidd's experiments, there is a large difference by several orders of magnitude in

451 viscosity between two simulations of different α when RH < 40%; for example, at 40% RH the

452 simulated SOA viscosity is $\sim 10^4$ Pa s with $\alpha = 1$, while it is $\sim 10^8$ Pa s with $\alpha = \alpha_{eff}$. The

453 contrasting response between the simulations of Kidd's and Renbaum-Wolff's experiments can

454 be explained by stark differences in SOA composition (see Fig. S1). This effect is caused by

455 different experimental setups and oxidant and precursor concentrations: Kidd et al. formed SOA

456 in a batch chamber with a low O_3/α-pinene ratio of 0.8, while Renbaum-Wolff et al. used a

457 continuous flow reactor with high O_3/α-pinene ratio of 3.

458   For the simulation of Kidd's experiments, ROOH and ROH compounds with relatively

459 large molar mass, high O:C ratio, and low volatility are formed at the early stage of reaction

460 followed by rapid condensation into the particle phase (Fig. S1, S2). The relatively low ozone

461 load limit further oxidation of ROOH and ROH compounds for fragmentation. Hence, SOA

462 has relatively high O:C ratio of 0.73 and low volatility, leading to very high viscosity and strong

463 reduction of α_{eff} (Fig. S5) to retard SOA growth. Consequently, the simulated SOA mass

464 loading is 15 μg m^{-3}, which is much lower than the simulation with $\alpha = 1$ (i.e., 7000 μg m^{-3}),

465 where higher volatility compounds would condense without kinetic limitations, resulting in

466 lower viscosity. The observed mass loadings in Kidd et al., 2014 were approximately ~1000 μg

467 m^{-3}. This indicates that particle viscosity and resulting kinetic limitations may be overestimated

468 in α_{eff} simulations or particle-phase reactions contribute substantially on SOA formation, as

469 discussed in Sect. 3.2.

470   For the simulation of Renbaum-Wolff's experiments, ROH compounds are the major

471 species formed in the gas phase during the first minutes of reaction (Fig. S1) and the continuous

472 input of O$_3$ leads to the fragmentation and decomposition of ROH species into RC(O)R

473 compounds with lower molar mass (Fig. S2, S3). Thus, SOA has relatively low O:C ratio of

474 0.49 and moderately low volatility (Fig. S4), resulting in lower viscosity compared to the case

475 of simulation for Kidd et al.. In this case, α_{eff} stays unity for low-volatile compounds ($C^0 < 10^{-2}$

476 μg m^{-3}), while it is reduced for semi-volatile compounds. The reduction of α of semi-volatile

477 compounds in α-pinene SOA has been recently observed by Liu et al. (2019), as shown in Fig.

478 S5. Note that, it is difficult to make a direct comparison between simulated and measured α_{eff}

479 due to the lack of detailed information on SOA formation conditions in Liu et al. (2019). The

480 mass loadings are on the same order being 15 and 79 μg m^{-3} for simulations with α_{eff} and $\alpha =$

481 1, respectively. Both results are close with the experimental measurement value of ~50 μg m^{-3}.

482 As viscosity measurements were not conducted at lower RH in Kidd et al. (2014) and time

483 evolution of SOA mass concentrations and viscosity are unavailable for both experimental

484 studies, it is hard to fully resolve impacts of mass accommodation in this study; we intend to

485 further investigate this aspect in a follow-up study.

486

487 **4. Conclusions**

488   We applied the T_g parameterizations and viscosity prediction method in the GECKO-A

489 box model to simulate the evolution of viscosity and composition of SOA generated via α-

490 pinene and isoprene oxidation. A range of simulations were performed with experimental

491 conditions applied for viscosity measurements in order to explore various effects such as

492 chemical composition, relative humidity, mass loadings, and mass accommodation coefficient

493 on SOA viscosity. Simulated viscosities are consistent with the observed RH-dependence of

494 viscosity for α-pinene and isoprene SOA, demonstrating the robustness of our viscosity

495 prediction method. Simulated viscosity values for isoprene SOA are in good agreement with

496 measurements, while those for α-pinene SOA were lower than experimental measurements by

497 a few orders of magnitude. The simulated chemical composition and functional group

498 distributions indicate that α-pinene SOA contain substantial amounts of aldehydes, ketones,

499 and carboxylic acids. These compounds are reactive and may undergo dimerization and

500 oligomerization reactions. In addition, GECKO-A does not treat detailed chemistry involving

501 stabilized Criegee intermediates, autoxidation and gas-phase dimerization by peroxy radicals.

502 These processes are known to lead to the formation of high molecular mass compounds that

503 would increase viscosity of SOA. Moreover, the model assumes that gas-particle partitioning

504 of organics follows Raoult's law with ideal mixing conditions. The implementation of these

505 processes is warranted in future studies for better representation of SOA chemical composition

506 and viscosity.

507 Experiments were conducted to form SOA under dry conditions followed by water

508 exposure for viscosity measurements and it was unnecessary to consider uptake of water into

509 the condensed phase upon SOA formation. Previous studies have suggested that water vapor

510 can significantly affect the composition of SOA. At higher RH water vapor interacts with

511 Criegee intermediates, leading to production of carboxylic acids or aldehydes and ketones via

512 decomposition routes (Kristensen et al., 2014). Kidd et al. (2014) have reported that as the RH

513 at which the SOA is formed increases, there is a decrease in viscosity, accompanied by an

514 increasing contribution from carboxylic acids and a decreasing contribution from higher

515 molecular mass products. These aspects including chemistry of Criegee intermediates and water

516 uptake should be a subject of future studies for simulating particle viscosity under humid

517 conditions.

518 We have also explored the effects of kinetic partitioning by accounting for reduction of

519 mass accommodation coefficient in a semisolid or viscous phase. The simulation results suggest

520 that kinetic limitations in the particle phase would result in a decrease in SOA mass loading

521 and an increase in viscosity due to suppression of condensation of semi-volatile compounds. It

522 is still challenging to accurately assess the extent of this effect on viscosity due to the lack of

523 experimental data for comparison and to the absence of some chemical processes in our

524 modeling method. Future experiments with simultaneous measurements of chemical

525 composition in the gas and particle phases as well as particle viscosity under different RH

526 conditions will be enormously helpful to further improve and constrain the model. While this

527 study simulated viscosity of pure organic particles, future studies should also investigate

528 viscosity of inorganic-organic particles and effects of non-ideal interactions including phase

529 separation (Zuend & Seinfeld, 2012; You et al., 2014) and gel formation (Richards et al., 2020).

530 The developed model in this study is a useful tool for further exploration of phase state of

531 atmospherically relevant SOA and it should also be useful in refining the representation of SOA

532 chemical evolution and phase state in regional and global air quality models.

533

534 **Acknowledgements.** MS acknowledges the Make Our Planet Great Again (MOPGA) short

535 stay program by the Campus France, which enabled MS to have a one-month research stay at

536 LISA hosted by BA in summer 2018. This work was also funded by the National Science

537 Foundation (AGS-1654104) and the Department of Energy (DE-SC0018349).

538

539 **Author contributions.** TG, BA, and MS designed the study. TG and MS conducted simulations

540 and data analysis. BA, RV, MC developed the GECKO-A and box models and provided a

541 training on the tools. YL developed the T_g parameterizations. TG and MS wrote the manuscript

542 with contributions from all coauthors.

543

544 **Competing interests.** The authors declare that they have no conflict of interest.

545

546 **Data availability.** Data and model outputs that are used for figures are available in CSV files

547 in the supplement.

548

549 **References.**

550 Aumont, B., Szopa, S. and Madronich, S.: Modelling the evolution of organic carbon during its
551 gas-phase tropospheric oxidation: development of an explicit model based on a self generating
552 approach, Atmos. Chem. Phys., 5, 2497-2517, 10.5194/acp-5-2497-2005, 2005.

553 Aumont, B., Szopa, S., and Madronich, S.: Modelling the evolution of organic carbon during
554 its gas-phase tropospheric oxidation: development of an explicit model based on a self
555 generating approach, Atmos. Chem. Phys., 5, 703–754, https://doi.org/10.5194/acpd-5-703-
556 2005, 2005.

557 Aumont, B., Valorso, R., Mouchel-Vallon, C., Camredon, M., Lee-Taylor, J., and Madronich,
558 S.: Modeling SOA formation from the oxidation of intermediate volatility n-alkanes, Atmos.
559 Chem. Phys., 12, 7577–7589, https://doi.org/10.5194/acp-12-7577-2012, 2012.

560 Bakker-Arkema, J. G. and Ziemann, P. J.: Measurements of Kinetics and Equilibria for the
561 Condensed Phase Reactions of Hydroperoxides with Carbonyls to Form Peroxyhemiacetals,
562 ACS Earth Sp. Chem., 4, 467–475, https://doi.org/10.1021/acsearthspacechem.0c00008, 2020.

Bateman, A. P., Bertram, A. K., and Martin, S. T.: Hygroscopic influence on the semisolid-to-liquid transition of secondary organic materials, J. Phys. Chem. A, 119, 4386–4395, https://doi.org/10.1021/jp508521c, 2015.

Bateman, A. P., Gong, Z., Harder, T. H., De Sá, S. S., Wang, B., Castillo, P., China, S., Liu, Y., O'Brien, R. E., Palm, B. B., Shiu, H. W., Cirino, G. G., Thalman, R., Adachi, K., Lizabeth Alexander, M., Artaxo, P., Bertram, A. K., Buseck, P. R., Gilles, M. K., Jimenez, J. L., Laskin, A., Manzi, A. O., Sedlacek, A., Souza, R. A.,Wang, J., Zaveri, R., and Martin, S. T.: Anthropogenic influences on the physical state of submicron particulate matter over a tropical forest, Atmos. Chem. Phys., 17, 1759–1773, https://doi.org/10.5194/acp-17-1759-2017, 2017.

Bates, K. H., Crounse, J. D., St. Clair, J. M., Bennett, N. B., Nguyen, T. B., Seinfeld, J. H., Stoltz, B. M., and Wennberg, P. O.: Gas phase production and loss of isoprene epoxydiols, J. Phys. Chem. A, 118, 1237–1246, https://doi.org/10.1021/jp4107958, 2014.

Berkemeier, T., Shiraiwa, M., Pöschl, U., and Koop, T.: Competition between water uptake and ice nucleation by glassy organic aerosol particles, Atmos. Chem. Phys., 14, 12513–12531, https://doi.org/10.5194/acp-14-12513-2014, 2014.

Bianchi, F., Kurtén, T., Riva, M., Mohr, C., Rissanen, M. P., Roldin, P., Berndt, T., Crounse, J. D., Wennberg, P. O., Mentel, T. F., Wildt, J., Junninen, H., Jokinen, T., Kulmala, M.,Worsnop, D. R., Thornton, J. A., Donahue, N., Kjaergaard, H. G., and Ehn, M.: Highly Oxygenated Organic Molecules (HOM) from Gas-Phase Autoxidation Involving Peroxy Radicals: A Key Contributor to Atmospheric Aerosol, Chem. Rev., 119, 3472–3509, https://doi.org/10.1021/acs.chemrev.8b00395, 2019.

Camredon, M., Aumont, B., Lee-Taylor, J., and Madronich, S.: The SOA/VOC/NOx system: an explicit model of secondary organic aerosol formation, Atmos. Chem. Phys, 7, 5599-5610, https://doi.org/10.5194/acp-7-5599-2007, 2007

Champion,W. M., Rothfuss, N. E., Petters, M. D., and Grieshop, A. P.: Volatility and Viscosity Are Correlated in Terpene Secondary Organic Aerosol Formed in a Flow Reactor, Environ. Sci. Technol. Lett., 6, 513–519, https://doi.org/10.1021/acs.estlett.9b00412, 2019.

Ciarelli, G., Colette, A., Schucht, S., Beekmann, M., Andersson, C., Manders-Groot, A., Mircea, M., Tsyro, S., Fagerli, H., Ortiz, A. G., Adani, M., Briganti, G., Cappelletti, A., D'Isidoro, M., Cuvelier, C., Couvidat, F., Meleux, F., and Bessagnet, B.: Long-term health impact assessment of total PM2.5 in Europe during the 1990–2015 period, Atmos. Environ. X, 3, 100032, https://doi.org/10.1016/j.aeaoa.2019.100032, 2019.

Davies, J. F. and Wilson, K. R.: Nanoscale interfacial gradients formed by the reactive uptake of OH radicals onto viscous aerosol surfaces, Chem. Sci., 6, 7020–7027, https://doi.org/10.1039/c5sc02326b, 2015.

Denjean, C., Formenti, P., Picquet-Varrault, B., Camredon, M., Pangui, E., Zapf, P., Katrib, Y., Giorio, C., Tapparo, A., Temime-Roussel, B., Monod, A., Aumont, B., and Doussin, J. F.: Aging of secondary organic aerosol generated from the ozonolysis of α-pinene: effects of ozone, light and temperature, Atmos. Chem. Phys., 15, 883-897, https://doi.org/10.5194/acp-15-883-2015, 2015.

603 DeRieux, W. S. W., Li, Y., Lin, P., Laskin, J., Laskin, A., Bertram, A. K., Nizkorodov, S. A.,
604 and Shiraiwa, M.: Predicting the glass transition temperature and viscosity of secondary organic
605 material using molecular composition, Atmos. Chem. Phys., 18, 6331–6351,
606 https://doi.org/10.5194/acp-18-6331-2018, 2018.

607 Dette, H. P., Qi, M., Schröder, D. C., Godt, A., and Koop, T.: Glass-forming properties of 3-
608 methylbutane-1,2,3-tricarboxylic acid and its mixtures with water and pinonic acid, J. Phys.
609 Chem. A, 118, 7024–7033, https://doi.org/10.1021/jp505910w, 2014.

610 Ditto, J. C., Joo, T., Khare, P., Sheu, R., Takeuchi, M., Chen, Y., Xu, W., Bui, A. A. T., Sun,
611 Y., Ng, N. L., and Gentner, D. R.: Effects of Molecular-Level Compositional Variability in
612 Organic Aerosol on Phase State and Thermodynamic Mixing Behavior, Environ. Sci. Technol.,
613 53, 13 009–13 018, https://doi.org/10.1021/acs.est.9b02664, 2019.

614 Donahue, N. M., Epstein, S. A., Pandis, 375 S. N., and Robinson, A. L.: A two-dimensional
615 volatility basis set: 1. organic-aerosol mixing thermodynamics, Atmos. Chem. Phys., 11, 3303–
616 3318, https://doi.org/10.5194/acp-11-3303-2011, 2011.

617 Evoy, E., Maclean, A. M., Rovelli, G., Li, Y., Tsimpidi, A. P., Karydis, V. A., Kamal, S.,
618 Lelieveld, J., Shiraiwa, M., Reid, J. P., and Bertram, A. K.: Predictions of diffusion rates of
619 large organic molecules in secondary organic aerosols using the Stokes-Einstein and fractional
620 Stokes-Einstein relations, Atmos. Chem. Phys., 19, 10073–10085, https://doi.org/10.5194/acp-
621 19-10073-2019, 2019.

622 Gervasi, N. R., Topping, D. O. and Zuend, A.: A predictive group-contribution model for the
623 viscosity of aqueous organic aerosol, Atmos. Chem. Phys., doi:10.5194/acp-20-2987-2020,
624 2020.

625 Grayson, J. W., Zhang, Y., Mutzel, A., Renbaum-Wolff, L., Böge, O., Kamal, S., Herrmann,
626 H., Martin, S. T., and Bertram, A. K.: Effect of varying experimental conditions on the viscosity
627 of α-pinene derived secondary organic material, Atmos. Chem. Phys., 16, 6027–6040,
628 https://doi.org/10.5194/acp-16-6027-2016, 2016.

629 Hinks, M. L., Brady, M. V., Lignell, H., Song, M., Grayson, J. W., Bertram, A. K., Lin, P.,
630 Laskin, A., Laskin, J., and Nizkorodov, S. A.: Effect of viscosity on photodegradation rates in
631 complex secondary organic aerosol materials, Phys. Chem. Chem. Phys., 18, 8785–8793,
632 https://doi.org/10.1039/c5cp05226b, 2016.

633 Hosny, N. A., Fitzgerald, C., Vyšniauskas, A., Athanasiadis, A., Berkemeier, T., Uygur, N.,
634 Pöschl, U., Shiraiwa, M., Kalberer, M., Pope, F. D., and Kuimova, M. K.: Direct imaging of
635 changes in aerosol particle viscosity upon hydration and chemical aging, Chem. Sci., 7, 1357–
636 1367, https://doi.org/10.1039/c5sc02959g, 2016.

637 Jain, S., Fischer, K. B., and Petrucci, G. A.: The influence of absolute mass loading of secondary
638 organic aerosols on their phase state, Atmosphere, 9, 131,
639 https://doi.org/10.3390/atmos9040131, 2018.

640 Jenkin, M. E., Valorso, R., Aumont, B., Rickard, A. R., andWallington, T. J.: Estimation of rate
641 coefficients and branching ratios for gas-phase reactions of OH with aliphatic organic
642 compounds for use in automated mechanism construction, Atmos. Chem. Phys., 18, 9297–
643 9328, https://doi.org/10.5194/acp-18-9297-2018, 2018a.

Jenkin, M. E., Valorso, R., Aumont, B., Rickard, A. R., andWallington, T. J.: Estimation of rate coefficients and branching ratios for gas-phase reactions of OH with aromatic organic compounds for use in automated mechanism construction, Atmos. Chem. Phys., 18, 9329–9349, https://doi.org/10.5194/acp-18-9329-2018, 2018b.

Jenkin, M. E., Valorso, R., Aumont, B., Newland, M. J., and Rickard, A. R.: Estimation of rate coefficients for the reactions of O3 with unsaturated organic compounds for use in automated mechanism construction, Atmos. Chem. Phys., 20, 12921-12937, https://doi.org/10.5194/acp-20-12921-2020, 2020.

Jenkin, M. E., Valorso, R., Aumont, B., and Rickard, A. R.: Estimation of rate coefficients and branching ratios for reactions of organic peroxy radicals for use in automated mechanism construction, Atmos. Chem. Phys., 19, 7691–7717, https://doi.org/10.5194/acp-19-7691-2019, 2019.

Jimenez, J. L., Canagaratna, M. R., Donahue, N. M., Prevot, A. S., Zhang, Q., Kroll, J. H., DeCarlo, P. F., Allan, J. D., Coe, H., Ng, N. L., Aiken, A. C., Docherty, K. S., Ulbrich, I. M., Grieshop, A. P., Robinson, A. L., Duplissy, J., Smith, J. D., Wilson, K. R., Lanz, V. A., Hueglin, C., Sun, Y. L., Tian, J., Laaksonen, A., Raatikainen, T., Rautiainen, J., Vaattovaara, P., Ehn, M., Kulmala, M., Tomlinson, J. M., Collins, D. R., Cubison, M. J., Dunlea, E. J., Huffman, J. A., Onasch, T. B., Alfarra, M. R., Williams, P. I., Bower, K., Kondo, Y., Schneider, J., Drewnick, F., Borrmann, S., Weimer, S., Demerjian, K., Salcedo, D., Cottrell, L., Griffin, R., Takami, A., Miyoshi, T., Hatakeyama, S., Shimono, A., Sun, J. Y., Zhang, Y. M., Dzepina, K., Kimmel, J. R., Sueper, D., Jayne, J. T., Herndon, S. C., Trimborn, A. M., Williams, L. R., Wood, E. C., Middlebrook, A. M., Kolb, C. E., Baltensperger, U., and Worsnop, D. R.: Evolution of organic aerosols in the atmosphere, Science (80-.)., 326, 1525–1529, https://doi.org/10.1126/science.1180353, 2009.

Julin, J., Winkler, P. M., Donahue, N. M., Wagner, P. E., and Riipinen, I.: Near-unity mass accommodation coefficient of organic molecules of varying structure, Environ. Sci. Technol., 48, 12 083–12 089, https://doi.org/10.1021/es501816h, 2014.

Kidd, C., Perraud, V., Wingen, L. M., and Finlayson-Pitts, B. J.: Integrating phase and composition of secondary organic aerosol from the ozonolysis of α-pinene, Proc. Natl. Acad. Sci. U.S.A., 111, 7552–7557, https://doi.org/10.1073/pnas.1322558111, 2014.

Knopf, D. A., Alpert, P. A., and Wang, B.: The Role of Organic Aerosol in Atmospheric Ice Nucleation: A Review, ACS Earth Sp. Chem., 2, 168–202, https://doi.org/10.1021/acsearthspacechem.7b00120, 2018.

Koop, T., Bookhold, J., Shiraiwa, M., and Pöschl, U.: Glass transition and phase state of organic compounds: Dependency on molecular properties and implications for secondary organic aerosols in the atmosphere, Phys. Chem. Chem. Phys., 13, 19 238–19 255, https://doi.org/10.1039/c1cp22617g, 2011.

Kristensen, K., Cui, T., Zhang, H., Gold, A., Glasius, M., and Surratt, J. D.: Dimers in α-pinene secondary organic aerosol: Effect of hydroxyl radical, ozone, relative humidity and aerosol acidity, Atmos. Chem. Phys., 14, 4201–4218, https://doi.org/10.5194/acp-14-4201-2014, 2014.

685 Kroll, J. H. and Seinfeld, J. H.: Chemistry of secondary organic aerosol: Formation and
686 evolution of low-volatility organics in the atmosphere, Atmos. Environ., 42, 3593–3624,
687 https://doi.org/10.1016/j.atmosenv.2008.01.003, 2008.

688 Kuwata, M. and Martin, S. T.: Phase of atmospheric secondary organic material affects its
689 reactivity, Proc. Natl. Acad. Sci. U.S.A., 109, 17354–17359,
690 https://doi.org/10.1073/pnas.1209071109, 2012.

691 La, Y. S., Camredon, M., Ziemann, P. J., Valorso, R., Matsunaga, A., Lannuque, V., Lee-
692 Taylor, J., Hodzic, A., Madronich, S., and Aumont, B.: Impact of chamber wall loss of gaseous
693 organic compounds on secondary organic aerosol formation: Explicit modeling of SOA
694 formation from alkane and alkene oxidation, Atmos. Chem. Phys., 16, 1417–1431,
695 https://doi.org/10.5194/acp-16-1417-2016, 2016.

696 Lambe, A. T., Onasch, T. B., Massoli, P., Croasdale, D. R., Wright, J. P., Ahern, A. T.,
697 Williams, L. R., Worsnop, D. R., Brune, W. H., and Davidovits, P.: Laboratory studies of the
698 chemical composition and cloud condensation nuclei (CCN) activity of secondary organic
699 aerosol (SOA) and oxidized primary organic aerosol (OPOA), Atmos. Chem. Phys., 11, 8913–
700 8928, https://doi.org/10.5194/acp-11-8913-2011, 2011.

701 Lee-Taylor, J., Madronich, S., Aumont, B., Baker, A., Camredon, M., Hodzic, A., Tyndall, G.
702 S., Apel, E., and Zaveri, R. A.: Explicit modeling of organic chemistry and secondary organic
703 aerosol partitioning for Mexico City and its outflow plume, Atmos. Chem. Phys., 11, 13 219–
704 13 241, https://doi.org/10.5194/acp-11-13219-2011, 2011.

705 Li, Y. and Shiraiwa, M.: Timescales of Secondary Organic Aerosols to Reach Equilibrium at
706 Various Temperatures and Relative Humidities, Atmos. Chem. Phys., 19, 5959–5971,
707 https://doi.org/10.5194/acp-19-5959-2019, 2019.

708 Li, Y., Day, D., Stark, H., Jimenez, J., and Shiraiwa, M.: Predictions of the glass transition
709 temperature and viscosity of organic aerosols from volatility distributions, Atmos. Chem. Phys.,
710 20, 8103–8122, https://doi.org/10.5194/acp-20-8103-2020, 2020.

711 Lim, Y. B. and Ziemann, P. J.: Effects of molecular structure on aerosol yields from OH radical-
712 initiated reactions of linear, branched, and cyclic alkanes in the presence of NOx, Environ. Sci.
713 Technol., 43, 2328–2334, https://doi.org/10.1021/es803389s, 2009.

714 Liu, X., Day, D. A., Krechmer, J. E., Brown, W., Peng, Z., Ziemann, P. J., and Jimenez, J. L.:
715 Direct measurements of semivolatile organic compound dynamics show near-unity mass
716 accommodation coefficients for diverse aerosols, Commun. Chem., 2, 98,
717 https://doi.org/10.1038/s42004-019-0200-x, 2019.

718 Maclean, A. M., Smith, N. R., Li, Y., Huang, Y., Hettiyadura, A. P. S., Crescenzo, G. V.,
719 Shiraiwa, M., Laskin, A., Nizkorodov, S. A. and Bertram, A. K.: Humidity-Dependent
720 Viscosity of Secondary Organic Aerosol from Ozonolysis of β-Caryophyllene: Measurements,
721 Predictions, and Implications, ACS Earth Sp. Chem., 5, 305-318, 2021.

722 Mai, H., Shiraiwa, M., Flagan, R. C., and Seinfeld, J. H.: Under What Conditions Can
723 Equilibrium Gas-Particle Partitioning Be Expected to Hold in the Atmosphere?, Environ. Sci.
724 Technol., 49, 11 485–11 491, https://doi.org/10.1021/acs.est.5b02587, 2015.

Marshall, F. H., Berkemeier, T., Shiraiwa, M., Nandy, L., Ohm, P. B., Dutcher, C. S., and Reid, J. P.: Influence of particle viscosity on mass transfer and heterogeneous ozonolysis kinetics in aqueous-sucrose-maleic acid aerosol, Phys. Chem. Chem. Phys., 20, 15 560–15 573, https://doi.org/10.1039/c8cp01666f, 2018.

McVay, R. C., Zhang, X., Aumont, B., Valorso, 445 R., Camredon, M., La, Y. S., Wennberg, P. O., and Seinfeld, J. H.: SOA formation from the photooxidation of α-pinene: Systematic exploration of the simulation of chamber data, Atmos. Chem. Phys., 16, 2785–2802, https://doi.org/10.5194/acp-16-2785-2016, 2016.

Mikhailov, E., Vlasenko, S., Martin, S. T., Koop, T., and Pöschl, U.: Amorphous and crystalline aerosol particles interacting with water vapor: Conceptual framework and experimental evidence for restructuring, phase transitions and kinetic limitations, Atmos. Chem. Phys., 9, 9491–9522, https://doi.org/10.5194/acp-9-9491-2009, 2009.

Mouchel-Vallon, C., Brauer, P., Camredon, M., Valorso, R., Madronich, S., Herrmann, H., and Aumont. B., Explicit modeling of volatile organic compounds partitioning in the atmospheric aqueous phase. Atmos. Chem. Phys., 13, 1023-1037, https://doi.org/10.5194/acp-13-1023-2013, 2013.

Nannoolal, Y., Rarey, J., and Ramjugernath, D.: Estimation of pure component properties part 3. Estimation of the vapor pressure of non-electrolyte organic compounds via group contribution and group interactions, Fluid Phase Equilib., 269, 117–133, https://doi.org/10.1016/j.fluid.2008.04.020, 2008.

Nozière, B., Kalberer, M., Claeys, M., Allan, J., D'Anna, B., Decesari, S., Finessi, E., Glasius, M., Grgi´c, I., Hamilton, J. F., Hoffmann, T., Iinuma, Y., Jaoui, M., Kahnt, A., Kampf, C. J., Kourtchev, I., Maenhaut, W., Marsden, N., Saarikoski, S., Schnelle-Kreis, J., Surratt, J. D., Szidat, S., Szmigielski, R., and Wisthaler, A.: The Molecular Identification of Organic Compounds in the Atmosphere: State of the Art and Challenges, Chem. Rev., 115, 3919–3983, https://doi.org/10.1021/cr5003485, 2015.

Pajunoja, A., Malila, J., Hao, L., Joutsensaari, J., Lehtinen, K. E., and Virtanen, A.: Estimating the viscosity range of SOA particles based on their coalescence time, Aerosol Sci. Technol., 48, https://doi.org/10.1080/02786826.2013.870325, 2014.

Paulot, F., Crounse, J. D., Kjaergaard, H. G., Kürten, A., Clair, J. M., Seinfeld, J. H., and Wennberg, P. O.: Unexpected epoxide formation in the gas-phase photooxidation of isoprene, Science (80-.)., 325, 730–733, https://doi.org/10.1126/science.1172910, 2009.

Peeters, J., Vereecken, L., and Fantechi, G.: The detailed mechanism of the OH-initiated atmospheric oxidation of α-pinene: A theoretical study, Phys. Chem. Chem. Phys., 3, 5489–5504, https://doi.org/10.1039/b106555f, 2001.

Petters, M. D. and Kreidenweis, S. M.: A single parameter representation of hygroscopic growth and cloud condensation nucleus activity, Atmos. Chem. Phys., doi:10.5194/acp-7-1961-2007, 2007.

Petters, M. D. and Kreidenweis, S. M.: A single parameter representation of hygroscopic growth and cloud condensation nucleus activity - Part 3: Including surfactant partitioning,

Atmos. Chem. Phys., 13, 1081–1091, https://doi.org/www.atmos-chem-phys.net/7/1961/2007/, 2013.

Petters, S. S., Kreidenweis, S. M., Grieshop, A. P., Ziemann, P. J., and Petters, M. D.: Temperature- and Humidity-Dependent Phase States of Secondary Organic Aerosols, Geophys. Res. Lett., 46, 1005–1013, https://doi.org/10.1029/2018GL080563, 2019.

Pöschl, U. and Shiraiwa, M.: Multiphase Chemistry at the Atmosphere-Biosphere Interface Influencing Climate and Public Health in the Anthropocene, Chem. Rev., 115, 4440–4475, https://doi.org/10.1021/cr500487s, 2015.

Prenni, A. J., Petters, M. D., Kreidenweis, S. M., DeMott, P. J. and Ziemann, P. J.: Cloud droplet activation of secondary organic aerosol, J. Geophys. Res. Atmos., doi:10.1029/2006JD007963, 2007.

Reid, J. P., Bertram, A. K., Topping, D. O., Laskin, A., Martin, S. T., Petters, M. D., Pope, F. D., and Rovelli, G.: The viscosity of atmospherically relevant organic particles, Nat. Commun., 9, 956, https://doi.org/10.1038/s41467-018-03027-z, 2018.

Renbaum-Wolff, L., Grayson, J. W., Bateman, A. P., Kuwata, M., Sellier, M., Murray, B. J., Shilling, J. E., Martin, S. T., and Bertram, A. K.: Viscosity of α-pinene secondary organic material and implications for particle growth and reactivity, Proc. Natl. Acad. Sci. U.S.A., 110, 8014–8019, https://doi.org/10.1073/pnas.1219548110, 2013.

Richards, D. S., Trobaugh, K. L., Hajek-Herrera, J., Price, C. L., Sheldon, C. S., Davies, J. F., and Davis, R. D.: Ion-molecule interactions enable unexpected phase transitions in organic-inorganic aerosol, Sci. Adv., 6, eabb5643, https://doi.org/10.1126/sciadv.abb5643, 2020.

Riva, M., Chen, Y., Zhang, Y., Lei, Z., Olson, N. E., Boyer, H. C., Narayan, S., Yee, L. D., Green, H. S., Cui, T., Zhang, Z., Baumann, K., Fort, M., Edgerton, E., Budisulistiorini, S. H., Rose, C. A., Ribeiro, I. O., Oliveira, R. L., Dos Santos, E. O., Machado, C. M., Szopa, S., Zhao, Y., Alves, E. G., De Sá, S. S., Hu, W., Knipping, E. M., Shaw, S. L., Duvoisin Junior, S., De Souza, R. A., Palm, B. B., Jimenez, J. L., Glasius, M., Goldstein, A. H., Pye, H. O., Gold, A., Turpin, B. J., Vizuete, W., Martin, S. T., Thornton, J. A., Dutcher, C. S., Ault, A. P., and Surratt, J. D.: Increasing Isoprene Epoxydiol-to-Inorganic Sulfate Aerosol Ratio Results in Extensive Conversion of I norganic Sulfate to Organosulfur Forms: Implications for Aerosol Physicochemical Properties, Environ. Sci. Technol., 53, 8682–8694, https://doi.org/10.1021/acs.est.9b01019, 2019.

Rothfuss, N. E. and Petters, M. D.: Influence of Functional Groups on the Viscosity of Organic Aerosol, Environ. Sci. Technol., 51, 271–279, https://doi.org/10.1021/acs.est.6b04478, 2017.

Schum, S. K., Zhang, B., Dzepina, K., Fialho, P., Mazzoleni, C., and Mazzoleni, L. R.: Molecular and physical characteristics of aerosol at a remote free troposphere site: Implications for atmospheric aging, Atmos. Chem. Phys., 18, 14017–14036, https://doi.org/10.5194/acp-18-14017-2018, 2018.

Seinfeld, J. H. and Pandis, S. N.: Atmospheric Chemistry and Physics: From Air Pollution to Climate Change, 3rd edition, John Wiley, 2016.

Shiraiwa, M. and Pöschl, U.: Mass Accommodation and Gas-Particle Partitioning in Secondary Organic Aerosols: Dependence on Diffusivity, Volatility, Particle-phase Reactions, and Penetration Depth, Atmos. Chem. Phys., In press, https://doi.org/10.5194/acp-2020-536, 2021.

Shiraiwa, M., Ammann, M., Koop, T., and Pöschl, U.: Gas uptake and chemical aging of semisolid organic aerosol particles, Proc. Natl. Acad. Sci. U.S.A., 108, 11003–11008, https://doi.org/10.1073/pnas.1103045108, 2011.

Shiraiwa, M., Pfrang, C., Koop, T., and Pöschl, U.: Kinetic multi-layer model of gas-particle interactions in aerosols and clouds (KMGAP): Linking condensation, evaporation and chemical reactions of organics, oxidants and water, Atmos. Chem. Phys., 12, 2777–2794, https://doi.org/10.5194/acp-12-2777-2012, 2012.

Shiraiwa, M., Yee, L. D., Schilling, K. A., Loza, C. L., Craven, J. S., Zuend, A., Ziemann, P. J., and Seinfeld, J. H.: Size distribution dynamics reveal particle-phase chemistry in organic aerosol formation, Proc. Natl. Acad. Sci. U.S.A., 110, 11746–11750, https://doi.org/10.1073/pnas.1307501110, 2013.

Shiraiwa, M., Li, Y., Tsimpidi, A. P., Karydis, V. A., Berkemeier, T., Pandis, S. N., Lelieveld, J., Koop, T., and Pöschl, U.: Global distribution of particle phase state in atmospheric secondary organic aerosols, Nat. Commun., 8, 15002, https://doi.org/10.1038/ncomms15002, 2017.

Shrivastava, M., Cappa, C. D., Fan, J., Goldstein, A. H., Guenther, A. B., Jimenez, J. L., Kuang, C., Laskin, A., Martin, S. T., Ng, N. L., Petaja, T., Pierce, J. R., Rasch, P. J., Roldin, P., Seinfeld, J. H., Shilling, J., Smith, J. N., Thornton, J. A., Volkamer, R., Wang, J., Worsnop, D. R., Zaveri, R. A., Zelenyuk, A., and Zhang, Q.: Recent advances in understanding secondary organic aerosol: Implications for global climate forcing, Rev. Geophys., 55, 509–559, https://doi.org/10.1002/2016RG000540, 2017.

Slade, J. H., Shiraiwa, M., Arangio, A., Su, H., Pöschl, U., Wang, J., and Knopf, D. A.: Cloud droplet activation through oxidation of organic aerosol influenced by temperature and particle phase state, Geophys. Res. Lett., 44, 1583–1591, https://doi.org/10.1002/2016GL072424, 2017.

Slade, J. H., Ault, A. P., Bui, A. T., Ditto, J. C., Lei, Z., Bondy, A. L., Olson, N. E., Cook, R. D., Desrochers, S. J., Harvey, R. M., Erickson, M. H., Wallace, H. W., Alvarez, S. L., Flynn, J. H., Boor, B. E., Petrucci, G. A., Gentner, D. R., Griffin, R. J., and Shepson, P. B.: Bouncier Particles at Night: Biogenic Secondary Organic Aerosol Chemistry and Sulfate Drive Diel Variations in the Aerosol Phase in a Mixed Forest, Environ. Sci. Technol., 53, 4977–4987, https://doi.org/10.1021/acs.est.8b07319, 2019.

Smith, N. R., Crescenzo, G., Huang, Y., Hettiyadura, A. P. S., Siemens, K., Li, Y., Faiola, C. L., Laskin, A., Shiraiwa, M., Bertram, A. K., and Nizkorodov, S. A., Viscosity and liquid-liquid phase separation in healthy and stressed plant SOA, Environ. Sci. Atmos., 1, 140-153, 10.1039/D0EA00020E, 2021

Song, M., Liu, P. F., Hanna, S. J., Li, Y. J., Martin, S. T., and Bertram, A. K.: Relative humidity-dependent viscosities of isoprene derived secondary organic material and atmospheric implications for isoprene-dominant forests, Atmos. Chem. Phys., 15, 5145–5159, https://doi.org/10.5194/acp-15-5145-2015, 2015.

Song, M., Liu, P. F., Hanna, S. J., Zaveri, R. A., Potter, K., You, Y., Martin, S. T., and Bertram, A. K.: Relative humidity-dependent viscosity of secondary organic material from toluene photo-oxidation and possible implications for organic particulate matter over megacities, Atmos. Chem. Phys., 16, 8817–8830, https://doi.org/10.5194/acp-16-8817-2016, 2016.

Song, M., MacLean, A. M., Huang, Y., Smith, N. R., Blair, S. L., 520 Laskin, J., Laskin, A., DeRieux,W. S.W., Li, Y., Shiraiwa,M., Nizkorodov, S. A., and Bertram, A. K.: Liquid-liquid phase separation and viscosity within secondary organic aerosol generated from diesel fuel vapors, Atmos. Chem. Phys., 19, 12515–12529, https://doi.org/10.5194/acp-19-12515-2019, 2019.

Tröstl, J., Chuang,W. K., Gordon, H., Heinritzi, M., Yan, C., Molteni, U., Ahlm, L., Frege, C., Bianchi, F.,Wagner, R., Simon, M., Lehtipalo, K., Williamson, C., Craven, J. S., Duplissy, J., Adamov, A., Almeida, J., Bernhammer, A. K., Breitenlechner, M., Brilke, S., Dias, A., Ehrhart, S., Flagan, R. C., Franchin, A., Fuchs, C., Guida, R., Gysel,M., Hansel, A., Hoyle, C. R., Jokinen, T., Junninen, H., Kangasluoma, J., Keskinen, H., Kim, J., Krapf, M., Kürten, A., Laaksonen, A., Lawler, M., Leiminger, M., Mathot, S., Möhler, O., Nieminen, T., Onnela, A., Petäjä, T., Piel, F. M., Miettinen, P., Rissanen, M. P., Rondo, L., Sarnela, N., Schobesberger, S., Sengupta, K., Sipilä, M., Smith, J. N., Steiner, G., Tomè, A., Virtanen, A., Wagner, A. C., Weingartner, E., Wimmer, D., Winkler, P. M., Ye, P., Carslaw, K. S., Curtius, J., Dommen, J., Kirkby, J., Kulmala, M., Riipinen, I., Worsnop, D. R., Donahue, N. M., and Baltensperger, U.: The role of low-volatility organic compounds in initial particle growth in the atmosphere, Nature, 533, 527–531, https://doi.org/10.1038/nature18271, 2016.

Tsigaridis, K., Daskalakis, N., Kanakidou, M., Adams, P. J., Artaxo, P., Bahadur, R., Balkanski, Y., Bauer, S. E., Bellouin, N., Benedetti, A., Bergman, T., Berntsen, T. K., Beukes, J. P., Bian, H., Carslaw, K. S., Chin, M., Curci, G., Diehl, T., Easter, R. C., Ghan, S. J., Gong, S. L., Hodzic, A., Hoyle, C. R., Iversen, T., Jathar, S., Jimenez, J. L., Kaiser, J.W., Kirkevåg, A., Koch, D., Kokkola, H., H Lee, Y., Lin, G., Liu, X., Luo, G., Ma, X., Mann, G. W., Mihalopoulos, N., Morcrette, J. J., Müller, J. F., Myhre, G., Myriokefalitakis, S., Ng, N. L., O'donnell, D., Penner, J. E., Pozzoli, L., Pringle, K. J., Russell, L. M., Schulz, M., Sciare, J., Seland, Shindell, D. T., Sillman, S., Skeie, R. B., Spracklen, D., Stavrakou, T., Steenrod, S. D., Takemura, T., Tiitta, P., Tilmes, S., Tost, H., Van Noije, T., Van Zyl, P. G., Von Salzen, K., Yu, F.,Wang, Z.,Wang, Z., Zaveri, R. A., Zhang, H., Zhang, K., Zhang, Q., and Zhang, X.: The AeroCom evaluation and intercomparison of organic aerosol in global models, Atmos. Chem. Phys., 14, 10 845–10 895, https://doi.org/10.5194/acp-14-10845-2014, 2014.

Vaden, T. D., Imre, D., Beránek, J., Shrivastava, M., and Zelenyuk, A.: Evaporation kinetics and phase of laboratory and ambient secondary organic aerosol, Proc. Natl. Acad. Sci. U.S.A., 108, 2190–2195, https://doi.org/10.1073/pnas.1013391108, 2011.

Valorso, R., Aumont, B., Camredon, M., Raventos-Duran, T., Mouchel-Vallon, C., Ng, N. L., Seinfeld, J. H., Lee-Taylor, J., and Madronich, S.: Explicit modelling of SOA formation from α-pinene photooxidation: Sensitivity to vapour pressure estimation, Atmos. Chem. Phys., 11, 6895–6910, https://doi.org/10.5194/acp-11-6895-2011, 2011.

Vereecken, L. and Peeters, J.: Decomposition of substituted alkoxy radicals - Part I: A generalized structure-activity relationship for reaction barrier heights, Phys. Chem. Chem. Phys., 11, 9062–9074, https://doi.org/10.1039/b909712k, 2009.

888 Vereecken, L., Müller, J. F., and Peeters, J.: Low-volatility poly-oxygenates in the OH-initiated
889 atmospheric oxidation of α-pinene: Impact of non-traditional peroxyl radical chemistry, Phys.
890 Chem. Chem. Phys., 9, 5241–5248, https://doi.org/10.1039/b708023a, 2007.

891 Vereecken, L. and Nozière, B.: H migration in peroxy radicals under atmospheric conditions,
892 Atmos. Chem. Phys., 20, 7429–7458, https://doi.org/10.5194/acp-20-7429-2020, 2020.

893 Verwer, J. G.: Gauss–Seidel Iteration for Stiff ODES from Chemical Kinetics, SIAM J. Sci.
894 Comput., 15, 1243–1250, https://doi.org/10.1137/0915076, 1994.

895 Verwer, J. G., Blom, J. G., and Hundsdorfer, W.: An implicit-explicit approach for atmospheric
896 transport-chemistry problems, Appl. Numer. Math., 20, 191–209,
897 https://doi.org/10.1016/0168-9274(95)00126-3, 1996.

898 Virtanen, A., Joutsensaari, J., Koop, T., Kannosto, J., Yli-Pirilä, P., Leskinen, J., Mäkelä, J. M.,
899 Holopainen, J. K., Pöschl, U., Kulmala, M., Worsnop, D. R., and Laaksonen, A.: An amorphous
900 solid state of biogenic secondary organic aerosol particles, Nature, 467, 824–827,
901 https://doi.org/10.1038/nature09455, 2010.

902 Virtanen, A., Kannosto, J., Kuuluvainen, H., Arffman, A., Joutsensaari, J., Saukko, E., Hao, L.,
903 Yli-Pirilä, P., Tiitta, P., Holopainen, J. K., Keskinen, J., Worsnop, D. R., Smith, J. N., and
904 Laaksonen, A.: Bounce behavior of freshly nucleated biogenic secondary organic aerosol
905 particles, Atmos. Chem. Phys., 11, 8759–8766, https://doi.org/10.5194/acp-11-8759-2011,
906 2011.

907 Wennberg, P. O., Bates, K. H., Crounse, J. D., Dodson, L. G., McVay, R. C., Mertens, L. A.,
908 Nguyen, T. B., Praske, E., Schwantes, R. H., Smarte, M. D., St Clair, J. M., Teng, A. P., Zhang,
909 X., and Seinfeld, J. H.: Gas-phase reactions of isoprene and its major oxidation products, Chem.
910 Rev., 118, 3337–3390, https://doi.org/10.1021/acs.chemrev.7b00439, 2018.

911 Ye, Q., Robinson, E. S., Ding, X., Ye, P., Sullivan, R. C., and Donahue, N. M.: Mixing of
912 secondary organic aerosols versus relative humidity, Proc. Natl. Acad. Sci. U.S.A., 113, 12
913 649–12 654, https://doi.org/10.1073/pnas.1604536113, 2016.

914 Ye, Q., Upshur, M. A., Robinson, E. S., Geiger, F. M., Sullivan, R. C., Thomson, R. J., and
915 Donahue, N. M.: Following particle-particle mixing in atmospheric secondary organic aerosols
916 by using isotopically labeled terpenes, Chem, 4, 318–333,
917 https://doi.org/10.1016/j.chempr.2017.12.008, 2018.

918 You, Y., Smith, M. L., Song, M., Martin, S. T., and Bertram, A. K.: Liquid-liquid phase
919 separation in atmospherically relevant particles consisting of organic species and inorganic
920 salts, Int. Rev. Phys. Chem., 33, 43–77, https://doi.org/10.1080/0144235X.2014.890786, 2014.

921 Zaveri, R. A., Easter, R. C., Shilling, J. E., and Seinfeld, J. H.: Modeling kinetic partitioning of
922 secondary organic aerosol and size distribution dynamics: Representing effects of volatility,
923 phase state, and particle-phase reaction, Atmos. Chem. Phys., 14, 5153–5181,
924 https://doi.org/10.5194/acp-14-5153-2014, 2014.

925 Zaveri, R. A., Shilling, J. E., Zelenyuk, A., Liu, J., Bell, D. M., D'Ambro, E. L., Gaston, C. J.,
926 Thornton, J. A., Laskin, A., Lin, P., Wilson, J., Easter, R. C., Wang, J., Bertram, A. K., Martin,
927 S. T., Seinfeld, J. H., and Worsnop, D. R.: Growth kinetics and size distribution dynamics of

928 viscous secondary organic aerosol, Environ. Sci. Technol., 52, 1191–1199,
929 https://doi.org/10.1021/acs.est.7b04623, 2018.

930 Zaveri, R. A., Shilling, J. E., Zelenyuk, A., Zawadowicz, M. A., Suski, K., China, S., Bell, D.
931 M., Veghte, D., and Laskin, A.: Particle-phase diffusion modulates partitioning of semivolatile
932 organic compounds to aged secondary organic aerosol, Environ. Sci. Technol., 54, 2595–2605,
933 https://doi.org/10.1021/acs.est.9b05514, 2020.

934 Zhang, Y., Sanchez, M. S., Douet, C., Wang, Y., Bateman, A. P., Gong, Z., Kuwata, M.,
935 Renbaum-Wolff, L., Sato, B. B., Liu, P. F., Bertram, A. K., Geiger, F. M., and Martin, S. T.:
936 Changing shapes and implied viscosities of suspended submicron particles, Atmos. Chem.
937 Phys., 15, 7819–7829, https://doi.org/10.5194/acp-15-7819-2015, 2015.

938 Zhang, Y., Chen, Y., Lambe, A. T., Olson, N. E., Lei, Z., Craig, R. L., Zhang, Z., Gold, A.,
939 Onasch, T. B., Jayne, J. T., Worsnop, D. R., Gaston, C. J., Thornton, J. A., Vizuete, W., Ault,
940 A. P., and Surratt, J. D.: Effect of the aerosol-phase state on secondary organic aerosol
941 formation from the reactive uptake of isoprene-derived epoxydiols (IEPOX), Environ. Sci.
942 Technol. Lett., 5, 167–174, https://doi.org/10.1021/acs.estlett.8b00044, 2018.

943 Zhang, Y., Nichman, L., Spencer, P., Jung, J. I., Lee, A., Heffernan, B. K., Gold, A., Zhang, Z.,
944 Chen, Y., Canagaratna, M. R., Jayne, J. T., Worsnop, D. R., Onasch, T. B., Surratt, J. D.,
945 Chandler, D., Davidovits, P., and Kolb, C. E.: The cooling rate- and volatility- dependent glass-
946 forming properties of organic aerosols measured by broadband dielectric spectroscopy,
947 Environ. Sci. Technol., 53, 12 366–12 378, https://doi.org/10.1021/acs.est.9b03317, 2019.

948 Zhou, S., Hwang, B. C., Lakey, P. S., Zuend, A., Abbatt, J. P., and Shiraiwa, M.: Multiphase
949 reactivity of polycyclic aromatic hydrocarbons is driven by phase separation and diffusion
950 limitations, Proc. Natl. Acad. Sci. U.S.A., 116, 11658–11663,
951 https://doi.org/10.1073/pnas.1902517116, 2019.

952 Ziemann, P. J. and Atkinson, R.: Kinetics, products, and mechanisms of secondary organic
953 aerosol formation, Chem. Soc. Rev., 41, 6582–6605, https://doi.org/10.1039/c2cs35122f, 2012.

954 Zobrist, B., Marcolli, C., Pedernera, D. A., and Koop, T.: Do atmospheric aerosols form
955 glasses?, Atmos. Chem. Phys., 8, 5221–5244, https://doi.org/10.5194/acp-8-5221-2008, 2008.

956 Zuend, A. and Seinfeld, J. H.: Modeling the gas-particle partitioning of secondary organic
957 aerosol: The importance of liquid-liquid phase separation, Atmos. Chem. Phys., 12, 3857–3882,
958 https://doi.org/10.5194/acp-12-3857-2012, 2012.

959

960

961 **Table 1:** Experimental conditions simulated in the box model to explore α-pinene and

962 isoprene SOA viscosity, and simulated glass transition temperatures of dry SOA ($T_{g,org}$) and

963 the O:C ratio.

Study	O_3 (ppm)	α-pinene (ppm)	RH (%)	T (K)	t (min.)	Exp. setup*	$T_{g,org}$ (K)	O:C
Renbaum-Wolff et al., 2013	0.30	0.1	0.5	298	30	Continuous flow. PF-BM	275 K	0.49
Zhang et al., 2015	30	0.7	0.5	293	6	Batch exp., DMA	258 K	0.43
Zhang et al., 2015	30	0.7	0.5	293	1.5	Batch exp., DMA	263 K	0.44
Kidd et al., 2014	0.65	0.8	dry,	297	30	Batch exp., PI	266 K	0.44
Grayson et al., 2016	0.07	0.1	0.5	298	80	Continuous flow, PF-BM	284 K	0.55
Bateman et al., 2015	0.1	0.3	0.5	298	174	Continuous flow, R	275 K	0.48
	O_3 (ppm)	Isoprene (ppm)	RH (%)	T (K)	t (min.)	Exp. setup*	$T_{g,org}$ (K)	
Song et al., 2015	10	4	13.0	293.15	1.4	Continuous flow, PF-BM	260	1.0

964 * Poke Flow Bead Mobility (PF-BM), Differential Mobility Analyzer (DMA), Particle

965 Impactor (PI), Rebound impactor (R).

966

967
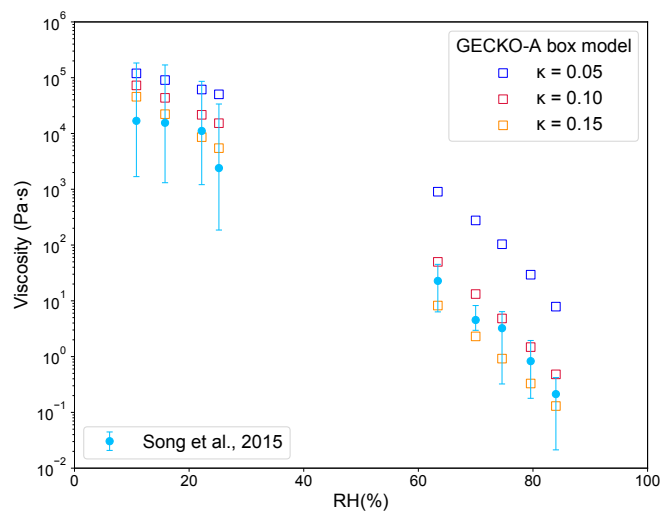
Figure 1: Viscosity of isoprene SOA as a function of RH. Circle markers with error bars represent measurements and associated uncertainties by Song et al. (2015) and square markers represent simulations with the GECKO-A box-model with different κ values.

971

972

973
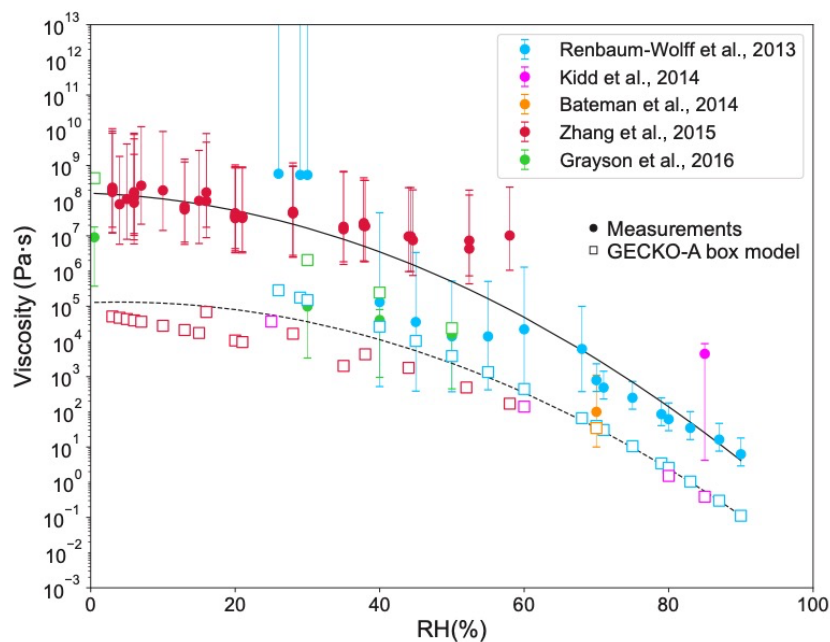
Figure 2: Comparison of measured (solid markers) and simulated (open markers) viscosity of
α-pinene SOA as a function of RH. For each set of laboratory experiments the measured
viscosities are reported with uncertainties. The solid and dashed lines represent the polynomial
regression for measurements and model simulations, respectively, to guide eyes.

978
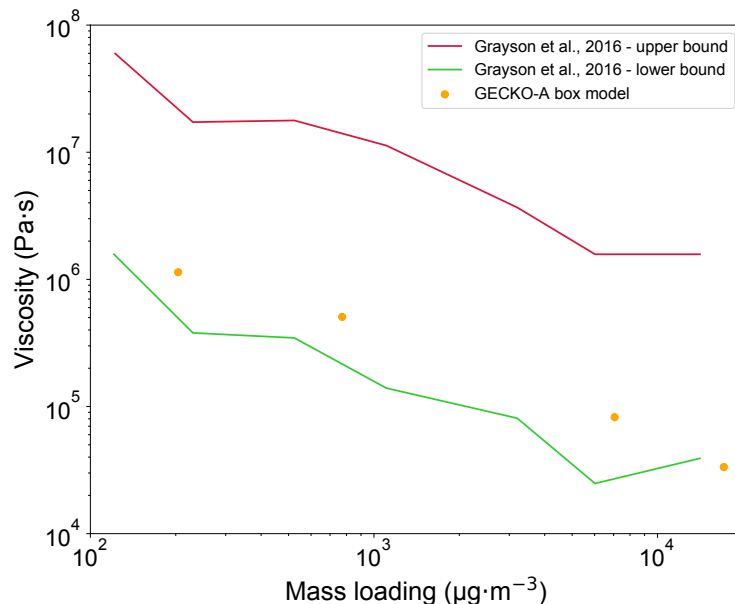
979
980 **Figure 3:** Impacts of SOA mass loadings on viscosity of α-pinene SOA. The red and green

981 lines represent the upper and lower bounds of measured viscosity in Grayson et al., 2016.

982 Orange markers represent simulated viscosities by the GECKO-A box model.

983
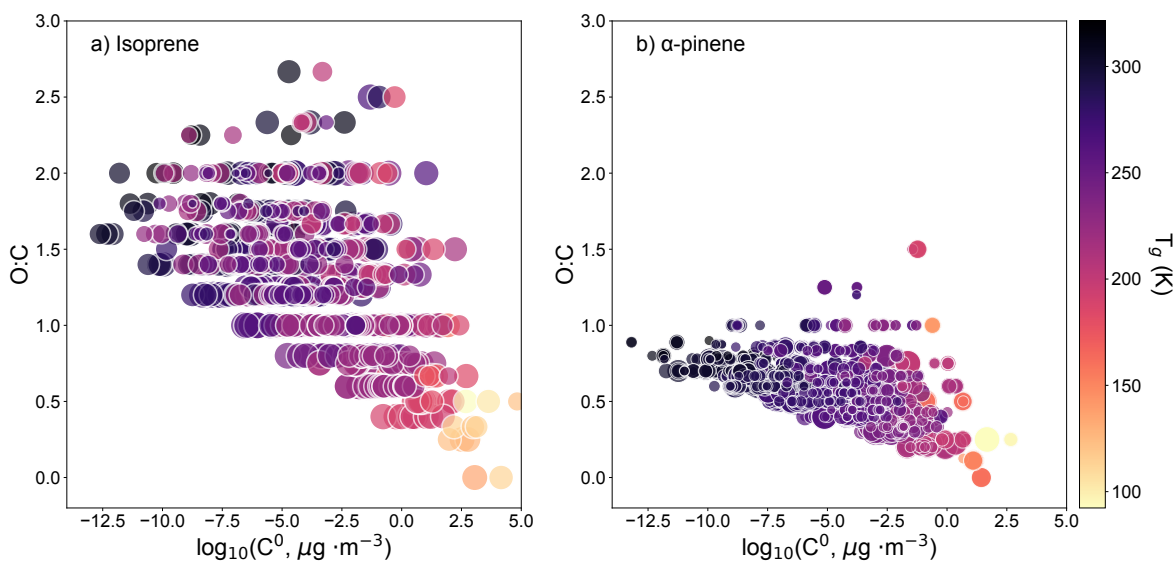
984
985 **Figure 4:** Chemical composition of SOA derived from oxidation of (a) isoprene and (b)

986 α-pinene of all simulated experimental conditions reported in Table 1 plotted in the 2D-VBS

987 framework of volatility and O:C ratio. Markers represent 500 most abundant particle-phase

988 compounds from each simulation. The markers are color-coded with T_g. The marker size is

989 scaled with particle phase concentration in each simulation.

990
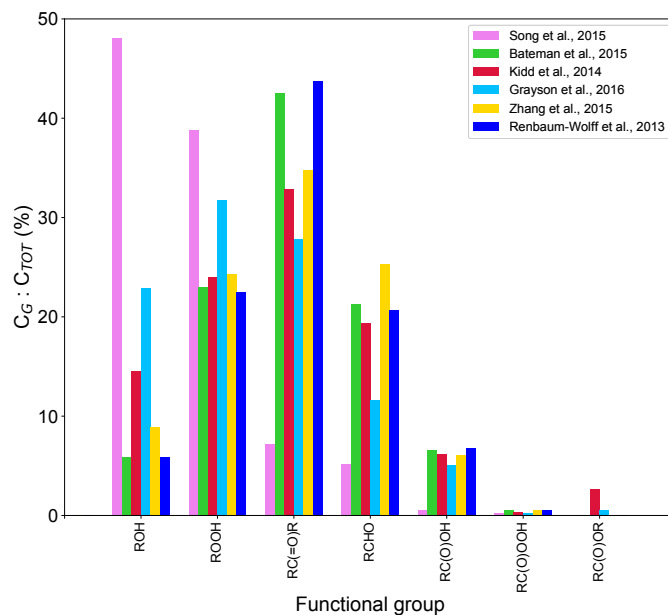
991

992 **Figure 5**: Simulated functional group distributions in particle-phase compounds derived from

993 isoprene photooxidation (Song et al., 2015) and α-pinene ozonolysis (Bateman et al., 2015;

994 Kidd et al., 2014; Grayson et al., 2016; Zhang et al., 2015; Renbaum-Wolff et al., 2013).

995

996
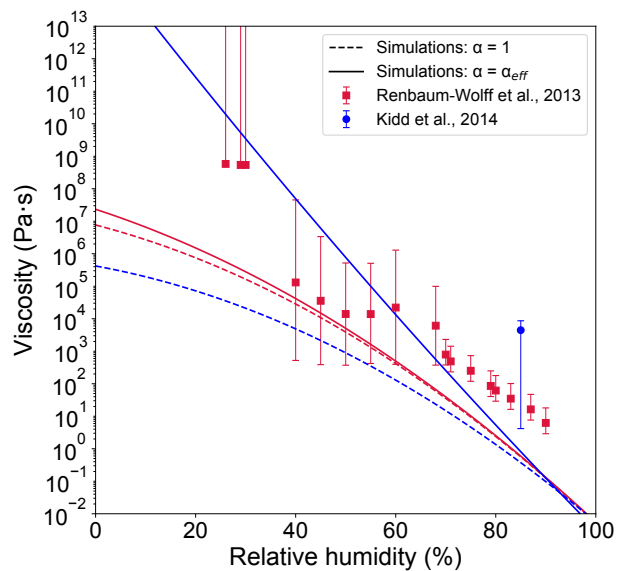
997 **Figure 6:** Simulated viscosities of α-pinene SOA with experimental conditions of Kidd et al.

998 (2014) (blue) and Renbaum-Wolff et al. (2013) (red). The simulations were conducted in two

999 different scenarios: α = 1 (dashed lines) and α = α$_{eff}$ (solid lines).

1000